Updated studies on the sensitivity of FCC-ee to heavy neutral leptons

Sarah Williams and John Hayward (University of Cambridge)

July 2024, updated March 2025 for FCC feasibility study

1 Introduction

As well as facilitating ultra-precise measurements of the Higgs, electroweak and top sectors of the Standard Model (SM) of particle physics, the electron-postron stage of the Future Circular Collider, FCC-ee, offers exciting opportunities to directly discover low-mass feebly interacting particles. In particular, searches for Long-Lived particles (LLPs) that couple to the Z and Higgs boson at the high-luminosity Z-pole and Zh runs benefit from ultra-high statistics and clean experimental conditions. This note focuses on searches for Heavy Neutral Leptons (HNLs) at the Z-pole run. HNLs are heavy, sterile neutrinos that occur in a number of Beyond-the Standard Model (BSM) solutions to the neutrino mass problem. Depending on the scenario they can be Dirac or Majorana and can mediate process that violate lepton flavour symmetries. If the HNLs mix with the SM neutrinos they can participate in weak interactions with couplings defined by $V_{\ell N_i}$ which are complex valued active-sterile mixing matrix element that describe the coupling between the heavy mass eigenstate i (with mass Ni) and the lepton flavour state ℓ. Depending on the mass and coupling the HNL decay can be prompt or long-lived, and when long-lived its decay can be targeted by reconstructing displaced vertices in the detector. Figure 1 shows representative diagrams for $e^+e^- \to Z \to L\nu_l$ at FCC-ee, with the HNL decaying to two leptons and a neutrino. Note that hadronic decays of the W and Z bosons can additionally give semi-leptonic and fully hadronic decay channels.

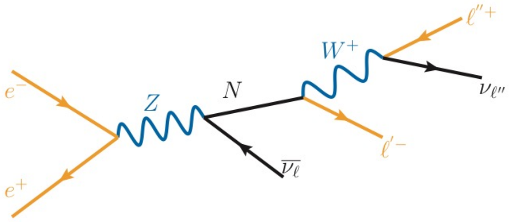

(a)

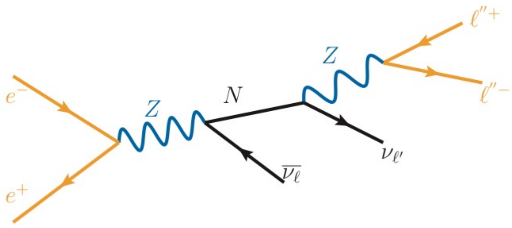

(b)

Figure 1: Representative diagrams for $e^+e^- \to Z \to L\nu_l$ at leading order, with the HNL decaying to two leptons and a neutrino via (a) charged current and (b) neutral current interactions.

For benchmarking purposes analyses often consider only the lightest neavy mass eigenstate N_1 (or just N) with mass m_N and mixings $V_{\ell N}$ though it should be noted that realistic scenarios typically contain multiple heavy mass eigenstates. Constraints can be placed on HNLs through a broad range of complementry techniques, from astrophysical measurements, to neutrino oscillation parameter measurements, electroweak precision observables, and direct searches at colliders and beam dump experiments. Figure 2 was compiled for the 2020 Update to the European strategy for particle physics, and summarises the sensitivity of various collider-based experiments along with the "Seesaw" limit, which gives the minimum lightest HNL mass to generate the neutrino masses through the Seesaw mechanism and the constraints from Big Bang Nucleosynthesis (BBN). The benchmark considered assumes a single HNL state which only couples to electrons.

For FCC-ee the "displaced vertex" search that is shown on the projections, comes from Ref. [2]. This considered all possible HNL decay channels (though the semileptonic has the highest branching ratio) and considered a search requiring that all visible particles inro the event emerge from the secondary vertex. The analysis argued that HNL decays with a vertex displacement between 10 μm and 249 cm could be detected in a background-free search (using the SiD detector [3]). The 2σ sensitivity contour was calculated based on signal models that would yield 4 events assuming 100% signal efficiency.

This note aims to provide updated projections on the sensitivity of the Z-pole run FCC-ee to HNLs using updated simulations of SM processes and detector concepts for FCC-ee. This will expand on work that was submitted as proceedings of the Snowmass 2021 community process in the US [4] and motivate further studies of the impact of choices of detector concepts on the physics sensitivity. As the bulk of this work was performed before the updates to the machine settings for FCC-ee that are being used for the final FCC feasibility study, which give 205 ab^{-1} at and around the Z pole (40 ab^{-1} at 87.9 GeV, 40 ab^{-1} at 94.3 GeV, 125 ab^{-1} at 91.2

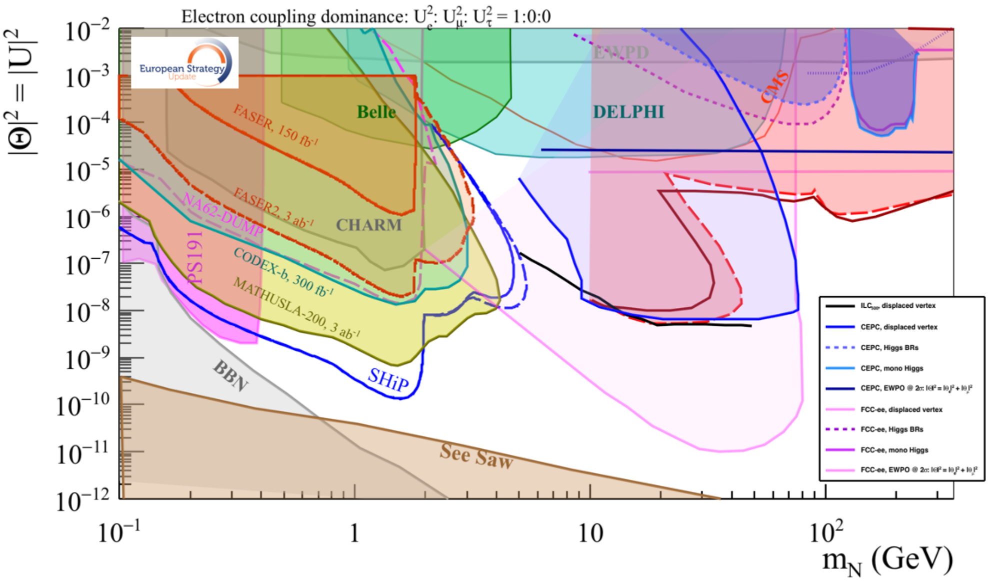

Figure 2: 90% exclusion limits for HNLs mixed with the electron neutrino, as presented in the Physics Briefing Book for the 2020 European Strategy Update [1]. The FCC-ee displaced vertex line was reproduced from Ref. [2]

GeV, for a total of about 6 $\times 10^{12}$ Z bosons), all of the plots and yields tables presented are for 150 ab^{-1} at the Z-pole, but the sensitivity projections in Section 6 are calculated for the correct normalisation of 6 $\times 10^{12}$ Z bosons.

2 Summary of previous work

The high-luminosity datasets at the Z-pole run and Zh threshold provide unique sensitivity to Beyond-the-Standard Model (BSM) particles with relative low mass and small couplings to the Z or Higgs boson. The high-statistics datasets at $\sqrt{s}$= 91 and 240 GeV, combined with the clean collision environments associated with e^+e^- collisions, enable background-free searches to be performed for particles including Heavy Neutral Leptons (HNLs), Axion-like particles (ALPs) and BSM particles that could be detected through exotic Higgs decays. The Snowmass white paper [4] studied HNL kinetics at particle level and presented initial detector level selections that exhibit significant background rejection whilst maintaining signal acceptance. Various HNL scenarios were simulated and the benchmark point yielding 1 expected signal event with 150 ab^{-1} of data was taken to be illustrative of the maximum sensitivity to long-lived HNLs that can be achieved at FCC-ee.

These initial results were performed using the first full simulation campaign within the FCC feasibility study. For the signal HNL samples the `Madgraph5_aMC@NLO` v3.2.0 event generator [5] was used to simulate at leading order parton-level e^+e^- collisions, with `Pythia` v8.303 [6] used to simulate the parton showering and hadronisation. The detector response was simulated using `Delphes` v3.4.2 [7] using a version of the Innovative Detector for Electron-positron Accelerators (IDEA) FCC-ee detector card [8]. Jets were reconstructed with `Fastjet` [9] with the anti-k_T algorithm with a cone size of 0.4, and the minimum p_T of constituents set to be 1 GeV. Events were stored in the common `EDM4HEP` event data format [10] which is a common data format used for simulation in future colliders. The raw number of events for the main backgrounds to HNL production are shown in Table 1 which also shows the "MC weight" applied to each raw event to scale to 150ab^{-1}. These demonstrate that ultimately these studies were limited by MC statistics, which have been extended in this study.

Process	Raw events in ref [4]	Cross-section in ref [4] [pb]	Sample luminosity [ab^{-1}]
Z$\rightarrow$ ee	10,000,000	1,462	0.01
Z$\rightarrow$ $\mu\mu$	10,000,000	1,462	0.01
Z$\rightarrow$ $\tau\tau$	10,000,000	1,477	0.01
Z$\rightarrow$ qq (q=u,d,s)	1,000,000,000	18,617	0.05
Z$\rightarrow$ cc	1,000,000,000	5,215	0.19
Z$\rightarrow$ bb	1,000,000,000	6,645	0.15

Table 1: The raw number of events, sample cross-section amd effective luminosity for the Monte Carlo samples used in Ref [4]. This paper performed the first detailed study of the potential sensitivity of FCC-ee to long-lived particles.

These samples also had several caveats that were subsequently identified, including an inefficiency in electron reconstruction due to the overlap removal procedure, and inconsistencies in the default jet collections stored in the EDM4HEP files. The issue with the jet collection arose from the applion of "overlap removal" (discussed further in the next section) in `Delphes` which led to all jets that contained π_0 particles in their shower being removed. Consequently, the impact of applying a jet veto to processes where multiple hadronic jets would be expected was not correctly quantified (and is likely to be conservative).

One result of the first study was the development of an event selection criteria designed to significantly suppress key background processes at the Z-pole whilst retaining signal efficiency to HNL benchmark models. The final selection included events with exactly two electrons (which are reconstructed down to 2 GeV in energy, with additional isolation criteria applied) and a veto on muons, photons and jets. To further suppress the backgrounds requirements were placed on the missing momentum $\not{p} > 10$ GeV and both electrons were required to have a transverse impact parameter $|d_0| > 0.5$ mm. This is the distance of the closest approach in the transverse plane of the helical trajectory of the track with respect to the beam axis and thus provides a measure of the reconstructed electron's displacement. Table 2 shows background and signal event yields, normalised to 150 ab^{-1} for these event selections as presented in Ref [4]. The errors presented are statistical only, and the numbers provided in brackets represent the total efficiency of that cut with respect to the total expected events (provided in the first column). Where no MC events passed the selection, inequalities are provided to represent possible uncertainties due to limited MC statistics.

$Z \rightarrow$	Total	Exactly 2 electrons	Vetoes	$\not{p} > 10$ GeV	Electron $\lvert d_0\rvert > 0.5$ mm	Rejection factor
ee	2.19 ± 10^{11}	1.85×10^{11} $\pm 6.19 \times 10^{7}$ (0.798)	1.53×10^{11} $\pm 5.8 \times 10^{7}$(0.698)	7.07×10^{8} $\pm 3.94 \times 10^{6}$ (0.003)	$\leq 3.94 \times 10^{-6}$ (< 0.001)	55,659.90
$\tau\tau$	2.22×10^{11}	5.49×10^{9} $\pm 1.10 \times 10^{7}$ (0.025)	5.10×10^{9} $\pm 1.06 \times 10^{7}$ (0.023)	2.52×10^{9} $\pm 7.47 \times 10^{6}$ (0.011)	6.64×10^{4} $\pm 3.84 \times 10^{4}$ (< 0.001)	3,336,596.39
uds	2.79×10^{12}	2.30×10^{7} $\pm 2.54 \times 10^{5}$ (< 0.001)	2.79×10^{3} $\pm 2.79 \times 10^{3}$	$\leq 2.79 \times 10^{3}$	$\leq 2.79 \times 10^{3}$	1,000,913,978.49
cc	7.82×10^{11}	1.69×10^{7} $\pm 1.21 \times 10^{5}$ (< 0.001)	5.22×10^{3} $\pm 2.13 \times 10^{3}$	1.74×10^{3} $\pm 1.23 \times 10^{3}$	$\leq 1.23 \times 10^{3}$	635,975,609.76
bb	9.97×10^{11}	5.64×10^{8} $\pm 9.85 \times 10^{5}$ (< 0.001)	3.25×10^{5} $\pm 2.36 \times 10^{4}$	1.22×10^{5} $\pm 1.45 \times 10^{4}$	1.72×10^{3} $\pm 1.72 \times 10^{3}$	579,505,813.95
$m_N, \lvert V_{eN}\rvert$						
10, 2×10^{-4}	2534	1006 ± 7 (0.397)	996 ± 7 (0.395)	951 ± 7 (0.375)	907 ± 7 (0.358)	2.79
20, 9×10^{-5}	458	313 ± 2 (0.683)	308 ± 2 (0.672)	293 ± 2 (0.640)	230 ± 1 (0.502)	1.99
20, 3×10^{-5}	51	34.7 ± 0.2 (0.680)	34.2 ± 0.2 (0.671)	32.6 ± 0.2 (0.639)	31.2 ± 0.2 (0.612)	1.63
30, 1×10^{-5}	5.01	3.85 ± 0.02 (0.768)	3.76 ± 0.02 (0.750)	3.54 ± 0.02 (0.707)	3.39 ± 0.02 (0.677)	1.48
50, 6×10^{-6}	1.23	0.99 ± 0.01 (0.805)	0.96 ± 0.01 (0.780)	0.92 ± 0.01 (0.748)	0.729 ± 0.004 (0.593)	1.69

Table 2: Expected numbers of events for signal and background processes, normalised to 150 ab^{-1}, for the event selection criteria identified in Ref [4]. The numbers in brackets represent the selection criteria of a cut relative to the total expected number of events. The final columnb provides the rejection factor (inverse of efficiency) for the full selection.

The significant background rejection whilst retaining signal acceptance was taken as supporting evidence that background-free searches could be performed for HNLS at FCC-ee. The benchmark point with HNL mass $m_N = 50$ GeV and mixing parameter $|V_{eN}| = 6 \times 10^{-6}$, which yielded around 1 event with 150 ab^{-1} was taken as illustrative of the maximum sensitivity to long-lived HNLs that could be achieved at FCC-ee. This study aims to extend this work both by implementing selections using updated Monte Carlo samples, and by considering additional selection criteria that could be used to extend the sensitivity.

3 Simulation and reconstruction details

One significant update in this work is the use of an updated set of Monte Carlo samples for the background modelling. The main changes relative to the first central production include an updated version of the `Delphes` detector card, with a smaller beam-pipe radius (R=1.0cm compared to R=1.5 previously) and improved resolution in the electromagnetic calorimeter (ECAL) through a crystal calorimeter. The machine parameters (beam energy spread and luminous region) are also updated to reflect developments on the accelerator studies. Table 3 summarises the number of events available in these samples, and (where applicable) gives the ratio to that used for the first study. For the leptonic Z-boson decays the statistics are increased by a factor of 10, where it is 5 and 4.39 respectively for $Z \rightarrow cc$ and $Z \rightarrow bb$ respectively. For this production a standalone $Z \rightarrow ss$ sample is also available. It should be noted that despite the larger statistics, the effective luminosity for all samples is still less than 1 ab^{-1}, meaning that this study will again be heavily limited by MC statistics.

In terms of the reconstructed quantities stored in the EDM4HEP files, the issue impacting the electron inefficiencies has been resolved and the default electrons and muon collections have no isolation criteria applied (the choice of which is then left to the analyser). To approximately account for bremstrahlung, the electron resolution is degraded relative to muons. Jet reconstruction is again performed through an interface to the `Fastjet` [9] package however the default jet collection stored is different and the choice of jet reconstruction algorithm used for targeting HNLs is reconsidered.

At hadron colliders like the LHC the longitudinal boost invariance about the beam drives jet algorithms to construct distance measures between jet constituents using p_T and $\Delta R_{ij} = \sqrt{\Delta\eta^2 + \Delta\phi^2}$. The `Anti-`$k_t$

Process	Raw events	Ratio to raw events in ref [4]	Cross-section [pb]
Z→ ee	100,000,000	10	1,462
Z→ $\mu\mu$	100,000,000	10	1,462
Z→ $\tau\tau$	100,000,000	10	1,477
Z→ qq (q=u,d)	497,658,654	−−	11,871
Z→ ss	499,842,440	−−	5,215
Z→ cc	499,786,495	5.00	5,215
Z→ bb	438,738,637	4.39	6,645

Table 3: The raw number of events, sample cross-section amd effective luminosity for the Monte Carlo samples used in this study.

algorithm [11] is a sequential recombination algorithm where the power of the energy scale in the distance measure is negative (-1). This has been the default algorithm at the LHC and was used in the Snowmass LLP white paper [4]. At e^+e^- colliders, the spherical symmetry associated with events means that energies and angles (θ_{ij}) between particle directions can be used in distance measures. Furthermore the absence of pileup and underlying event means that all hadrons should end up in a jet, which can be exploited in exclusive algorithms. One such example is the "exclusive Durham k_T" algorithm [12]. This sequentially recombines constituents i,j with the smallest distance measure d_{ij} (these are recalculated each time) and stops either when a pre-defined number of jets are reconstructed or when all remaining distances exceed a threshold. For the latter, if targeting a particular hadronic process a requirement on a minimum number of jets may be subsequently applied to the event. This reconstruction technique has great potential when combined with flavour tagging for processes such as $ZH(H \to bb)$, however for the HNL processes under consideration in this study the target signal has no jets in the final state, meaning that "inclusive" algorithms are a more natural choice for defining jet vetoes. The inclusive anti-k_T algorithm tends to produce "circular" jets where all constituents within some cone R are captured, and to retain infrared safety a minimum energy cut must be applied to the resulting jets. One aim of this study is to understand the impact on background rejection rates for different choices of inclusive jet algorithm.

In ref [4] background rejection was achieved through lower cuts on the reconstructed electron-track transverse impact parameters $|d_0| > 0.5$ mm in each event. This study aims to extend this and consider the impact of reconstructed secondary vertices in the event. Secondary vertices are reconstructed using `LCFIPlus` [13] framework. This builds on work by the the LCFIVertex collaboration within the Linear Collider community to provides tools for vertex finding and for identification of the flavour and charge of the leading hadron in heavy flavour jets. When selecting tracks to be passed through the secondary vertex reconstruction, an algorithm to suppress tracks from photon conversions and from decays of short-lived Λ and K_S hadrons is applied. The secondary vertex reconstruction then begins by finding a vertex seed, where every possible track pair is fitted to a vertex, and then the one that passes selection criteria with the lowest χ^2 is chosen as the vertex seed. Further tracks can then be added to this vertex; the track that forms a vertex with the lowest χ^2 with this seed vertex and passes track selection criteria is then added to this seed. This procedure continues until no more tracks pass the selection. This vertex is then stored, and all tracks associated with it are removed from the set of tracks, and the proceedure is then repeated until no more vertex seeds can be formed.

In this study, the default configuration for secondary vertex (SV) reconstruction considered tracks with $p_T > 1$ GeV and $|d_0| > 0.5$ mm to avoid reconstructed secondary vertices from prompt particle decays but to remain aligned with the d_0 cuts applied to electron tracks in the previous study. For the vertex seeds, the invariant mass of the two tracks must be less than 40 GeV and the χ^2 must be less than 9, and when adding additional tracks the χ^2 contribution of the track must be less than 5.

In the previous studies, the default reconstructed objects returned by `Delphes` (electrons, muons, jets) were used. For experiments that use independent algorithms to reconstruct different physics objects double counting can occur due to the signals from a single particle being reconstructed as more than one different object. To remove such ambiguities "overlap" removal procedures are typically applied that discard objects based on a pre-defined hierarchy for reconstructed objects. In this study overlap removal is emulated by re-running the jet clustering algorithms with the reconstructed electrons and muons removed from the list of the reconstructed particles used for clustering. The impact of this can be seen in Figure 3 which shows three jet multiplicity distribution for events with exactly two electrons, and no muons or photons. The first is the default jet collection for the new MC production, which uses a "generalised inclusive k_T" algorithm with a cone size $R = 1.5$, and the scale power $p = -1$ (as with anti-k_T) and a minimum p_T cut on constituents at 1 GeV. As this algorithm tends to capture all particles within an angle R, it is unsurprising that the distribution for $Z \to ee$ peaks at 2, which would correspond to both electrons being double counted also as jets. For the remainder of this study, the jet selections will be defined using the jet collection shown in (c), which corresponds to jets reconstructed using the anti-k_T algorithm with reconstructed leptons removed from the particles included in the clustering. The jet collections in (c) are used throughout the rest of this paper.

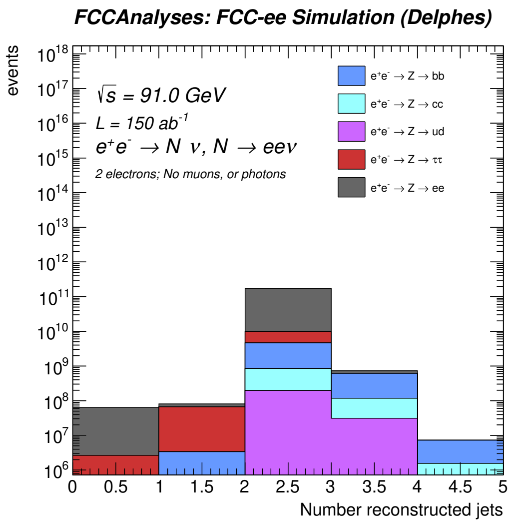

(a)

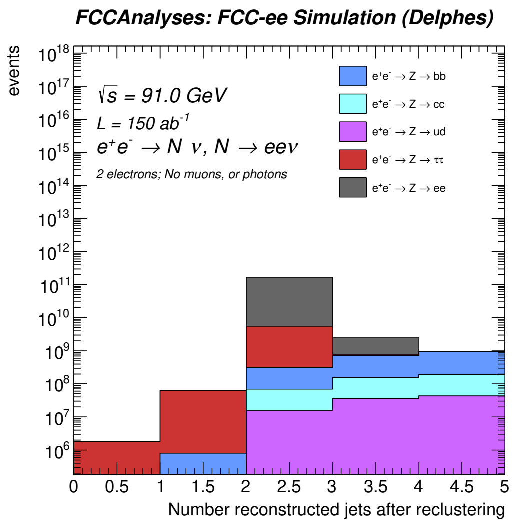

(b)

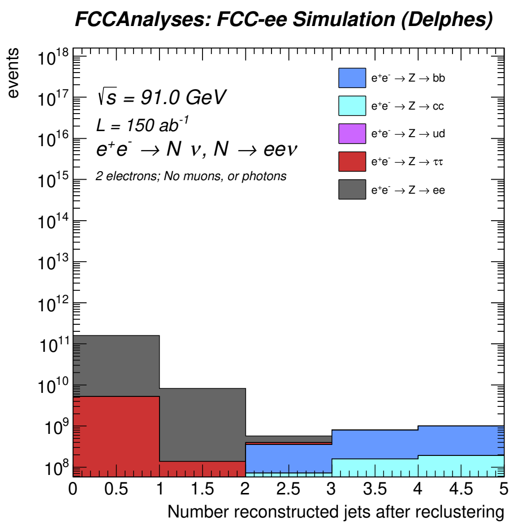

(c)

Figure 3: Jet multiplicity distributions for (a) the default jet collection stored in the `Delphes` samples (generalised k_T with $p = -1$ and a minimum p_T cut of 1 GeV), (b) jets reclustered using the anti-k_T algorithm with a minimum p_T cut of 1 GeV and (c) jets reclustered with the anti-k_T algorithm as in (b) but with all reconstructed leptons (electrons and muons) removed from the reclustering.

4 Event selections

The first step of this study is to recalculate the expected event yields at $150ab^{-1}$ to compare with the selections in the original study. These are presented in table 4. The efficiencies at the jet veto stage are approximately unchanged $Z \to ee$ and $Z \to \tau\tau$ as in the previous study, but for the hadronic decays the effiencies are much lower, reflecting the higher background efficiency now the jet reclustering is performed correctly. For the signal processes the efficiencies are much higher (between 80 and 95%) which is likely due to the recovery in electron efficiency at low p_T. Figure 4 shows the leading- and sub-leading- electron energy distributions after applying the event vetoes. The lightest HNL scenario which had the lowest efficiency after the jet veto in the Snowmass study (m_N=10 GeV) is flat in the sub-leading lepton at lower values, which could explain why the efficiency was significantly lower in the previous study.

Figure 5 shows the missing momentum distribution for events with two electrons and satisfying the veto on jets, muons and photons. The shapes are broadly similar to the previous study. The requirement of $\not{p} > 10$ GeV was motivated by the large peak into the $Z \to ee$ distribution towards 0. Above this cut, the $Z \to \tau\tau$ is the dominant background as illustrated in the yields in Table 4. Due to the neutrinos in the final state, a missing energy cut could still be beneficial to optimise for background rejection against signal acceptance but this is left for further studies with larger background samples.

Rather than cutting on the electron $|d_0|$, this study aims to consider requirements on the number of secondary vertices. The final column in Table 4 shows that, once the event vetoes have been required, an additional requirement of exactly 1 displaced vertex leaves no MC events for any background process (hence the upper limits). Figure 6 shows the distribution of secondary vertex multiplicity for events with two electrons, and no

$Z \to$	2 electrons	Veto photons and muons	Veto jets	Vetoes and $\not{p} > 10$GeV	Vetoes and 1 DV
ee	1.62e+11 ± 8.83e+08	1.62e+11 ± 1.89e+07	1.54e+11 ± 1.84e+07 (0.702)	3.21e+08 ± 8.39e+05	≲ 8.39e+05
$\tau\tau$	5.39e+09 ± 1.63e+08	5.39e+09 ± 3.46e+06	5.22e+09 ± 3.40e+06 (0.023)	2.57e+09 ± 2.39e+06	4.43e+03 ± 3.13e+03
bb	4.27e+09 ± 1.48e+08	4.27e+09 ± 3.11e+06	1.40e+06 ± 5.65e+04 (< 0.001)	4.29e+05 ± 3.12e+04	2.27e+03 ± 2.27e+03
cc	7.39e+08 ± 4.25e+07	7.39e+08 ± 1.08e+06	3.29e+04 ± 7.17e+03 (< 0.001)	1.10e+04 ± 4.14e+03	≲ 4.14e+03
ud	2.28e+08 ± 5.40e+07	2.28e+08 ± 9.03e+05	1.43e+04 ± 7.16e+03 (< 0.001)	1.07e+04 ± 6.20e+03	≲ 6.20e+03
ss	1.19e+08 ± 1.70e+07	1.19e+08 ± 4.31e+05	1.10e+04 ± 4.14e+03 (< 0.001)	3.13e+03 ± 2.21e+03	≲ 2.21e+03
$m_N, \lvert V_{eN} \rvert$					
10, 2×10^{-4}	2.04e+03 ± 2.29e+00	2.04e+03 ± 1.02e+01	2.04e+03 ± 1.02e+01 (0.805)	1.98e+03 ± 1.00e+01	1.89e+03 ± 9.77e+00
20, 9×10^{-5}	4.04e+02 ± 1.84e-01	4.04e+02 ± 1.92e+00	4.04e+02 ± 1.92e+00 (0.882)	3.87e+02 ± 1.88e+00	3.11e+02 ± 1.69e+00
20, 3×10^{-5}	4.44e+01 ± 6.77e-03	4.44e+01 ± 2.12e-01	4.43e+01 ± 2.12e-01 (0.869)	4.25e+01 ± 2.08e-01	4.18e+01 ± 2.06e-01
30, 1×10^{-5}	4.62e+00 ± 2.15e-04	4.62e+00 ± 2.15e-02	4.62e+00 ± 2.15e-02 (0.922)	4.37e+00 ± 2.09e-02	4.33e+00 ± 2.08e-02
50, 6×10^{-6}	1.17e+00 ± 2.67e-05	1.17e+00 ± 5.38e-03	1.17e+00 ± 5.38e-03 (0.952)	1.13e+00 ± 5.28e-03	7.89e-01 ± 4.41e-03

Table 4: Event yields, normalised to $150ab^{-1}$ for background and signal processes for event selection criteria taken from the snowmass study, but extended to consider the presence of displaced vertices. For comparison, the efficiency of the requirement of 2 electrons and a veto on photons, muons and jets is provided in brackets.

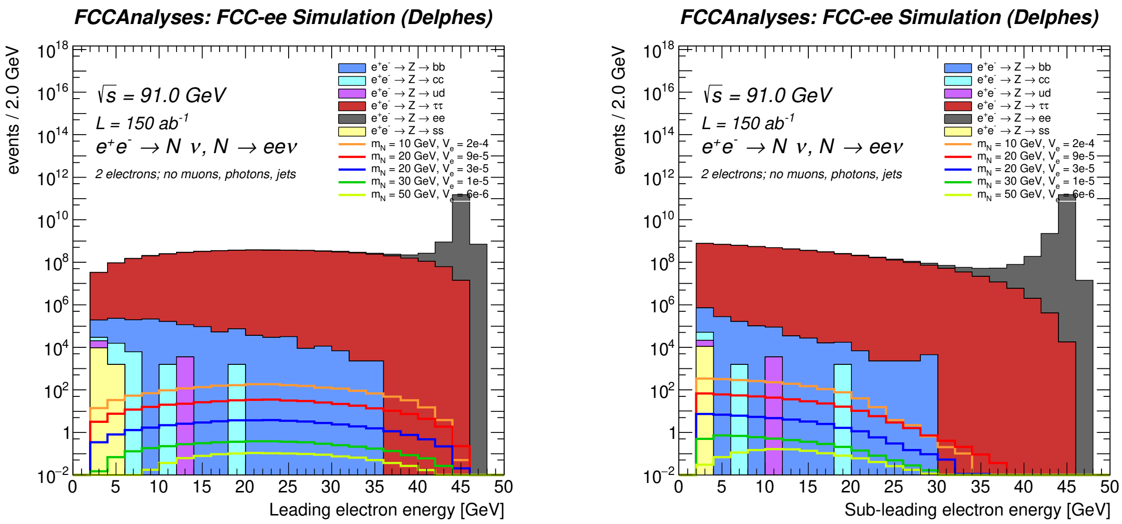

(a) (b)

Figure 4: (a) leading electron energy and (b) sub-leading electron energy distributions normalised to 150 ab^{-1}, for representative HNL benchmark points and the main Z-pole background processes. All events are required to have exactly two electrons, and no additional muons, jets or photons.

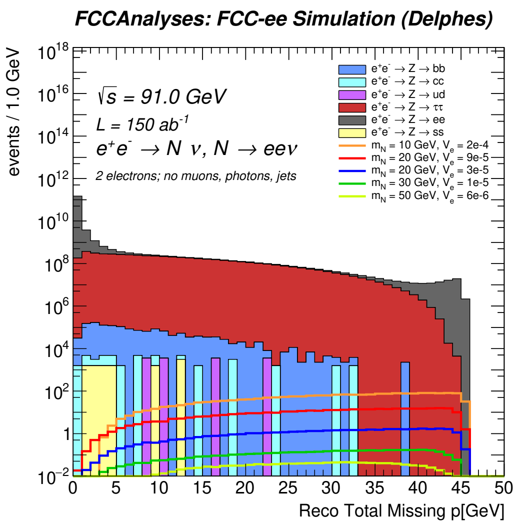

Figure 5: Reconstructed missing momentum distribution, normalised to 150 ab^{-1}, for representative HNL benchmark points and the main Z-pole background processes. All events are required to have exactly two electrons, and no additional muons, jets or photons.

muons or photons. Requiring exactly one displaced vertex will remove entirely the $Z \to ee$ backgrounds, and as illustrated in the final column of Table 4 the only processes with MC events remaining are $Z \to bb$ and $Z \to \tau\tau$

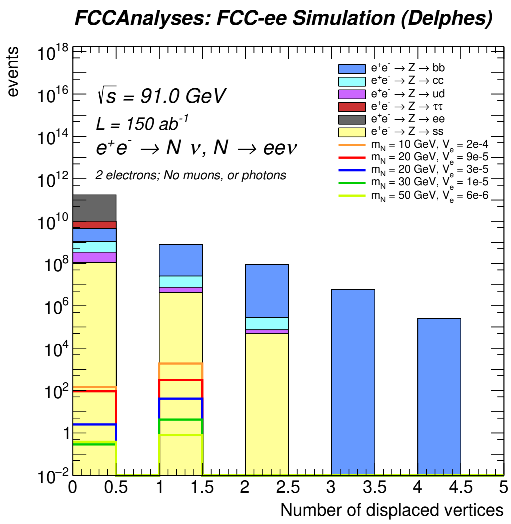

Figure 6: Distribution of the number of reconstructed secondary vertices (reconstructed with a track p_T cut of 1 GeV and a minimum $|d_0|$ requirement of 0.5 mm), normalised to 150 ab^{-1}, for representative HNL benchmark points and the main Z-pole background processes. All events are required to have exactly two electrons, and no additional muons or photons.

To investigate which variables could provide further discrimination between signal and background, Figure ?? presents a set of kinematic distributions for the signal and background, for all events with exactly two electrons, no photons or muons, and exactly one displaced vertex. The jet veto requirement is relaxed in order to increase statistics to see the shape of the distributions. Figure 7 provides the missing momentum and jet multiplicity distributions, and Figure 8 provides a set of kinematic distributions calculated using the two reconstructed electrons in the event including the dielectron invariant mass and several angular variables. Figure 9 provides distribution of the leading- and sub-leading electron energy and track $|d_0|$ and Figure 10 gives distributions of quantities related to the reconstructed secondary vertex (the reconstructed decay length, and its error and significance).

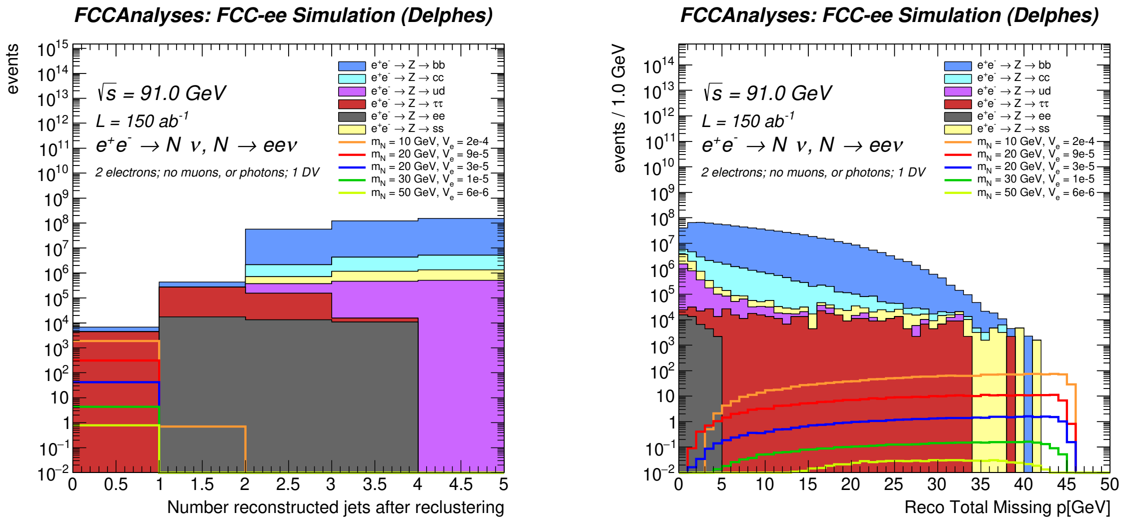

(a) (b)

Figure 7: Distributions, normalised to 150 ab^{-1}, of the (a) the jet multiplicity and (b) magnitude of the missing momentum, for background and benchmark HNL processes for events with exactly 2 electrons, no muons and photons and an additional requirement of exactly 1 reconstructed secondary vertex (reconstructed with a track p_T cut of 1 GeV and a minimum $|d_0|$ requirement of 0.5 mm).

Figure 7 further reinforces the observation that once the jet veto is applied, the dominant backgrounds are $Z \to bb$ and $Z \to \tau\tau$. The missing momentum distribution distributions for the signal peaks at higher values, however finding an optimised value for this cut would require higher MC statistics to look at the shapes of the distribution for the remaining backgrounds once the jet veto has been applied. Similarly, the distributions in Figure 8 could be further used to discriminate between signal and backgrounds, which also motivates further study.

To illustrate the challenge posed by limited MC statistics, Figure 11 provides distributions of the leading- and sub-leading electron track d_0, the di-electron invariant mass and the reconstructed decay length, for events with the jet veto and secondary vertex requirement applied. The shapes of the signal distribution are distinct, but the MC distributions contain only 3 events with weights of the order of 10^3. These results are taken as promising that with further background studies a background-free search could be constructed with significant sensitivity to HNLs. These studies will be performed through implementing generator-level filtering in the `Key4Hep` software stack to enable extreme topologies in rare corners of parameter space to be studied in event samples of the required statistics for FCC-ee.

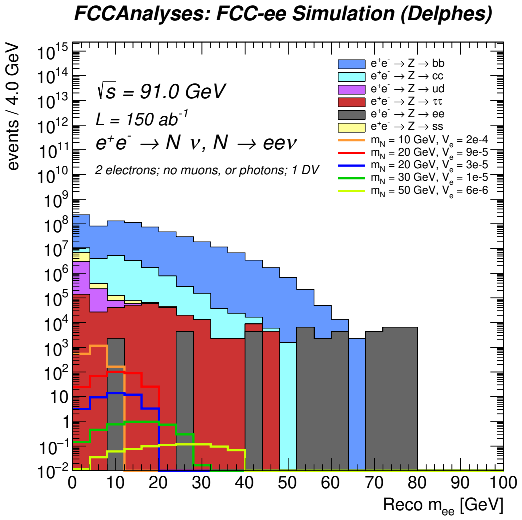

(a)

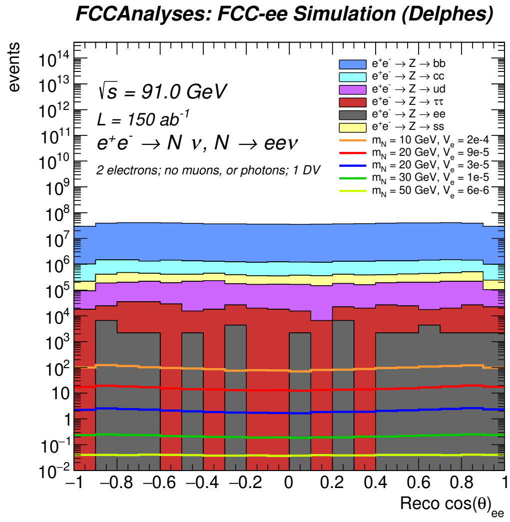

(b)

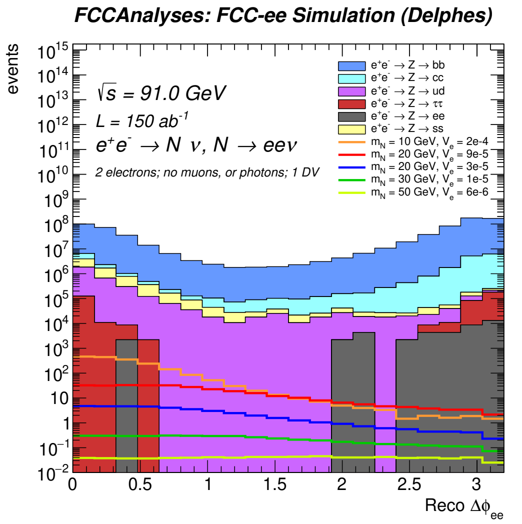

(c)

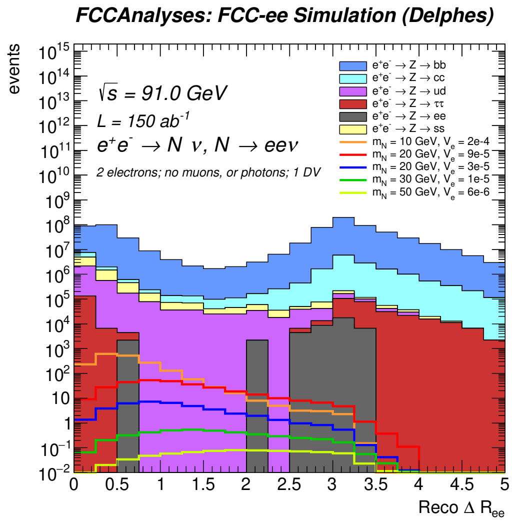

(d)

Figure 8: Distributions, normalised to 150 ab^{-1}, of the (a) di-electron invariant mass, (b) $\cos theta_{ll}$ for the dielectron system, (c) $\Delta\phi$ between the two electrons and (d) ΔR between the two electrons, for background and benchmark HNL processes for events with exactly 2 electrons, no muons and photons and an additional requirement of exactly 1 reconstructed secondary vertex (reconstructed with a track p_T cut of 1 GeV and a minimum $|d_0|$ requirement of 0.5 mm).

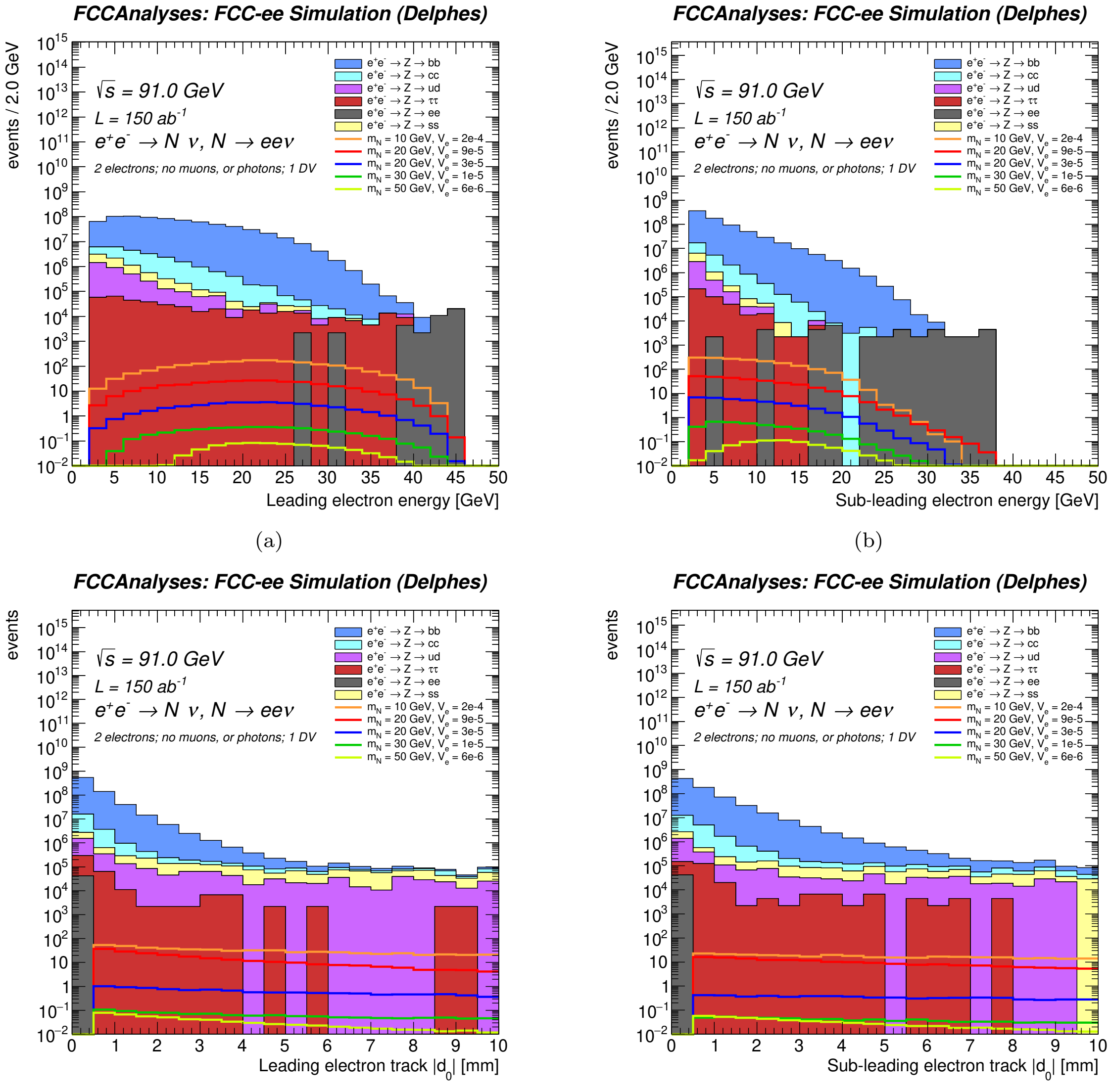

Figure 9: Distributions, normalised to 150 ab^{-1} for background and benchmark HNL processes for events with exactly 2 electrons, no muons and photons and an additional requirement of exactly 1 reconstructed secondary vertex (reconstructed with a track p_T cut of 1 GeV and a minimum $|d_0|$ requirement of 0.5 mm). (a) and (b) show the leading lepton energy and track $|d_0|$ and (c) and (d) show these distributions for the sub-leading electron.

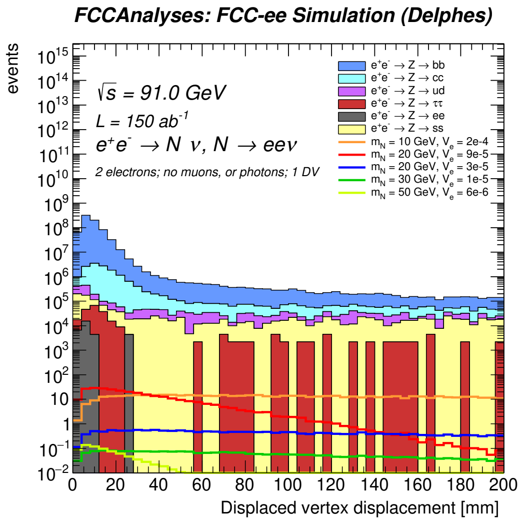

(a)

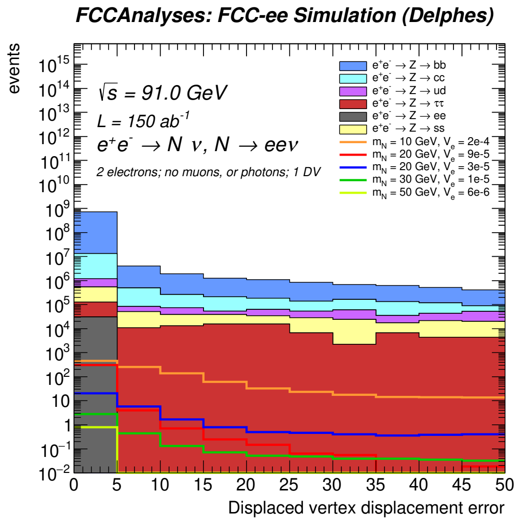

(b)

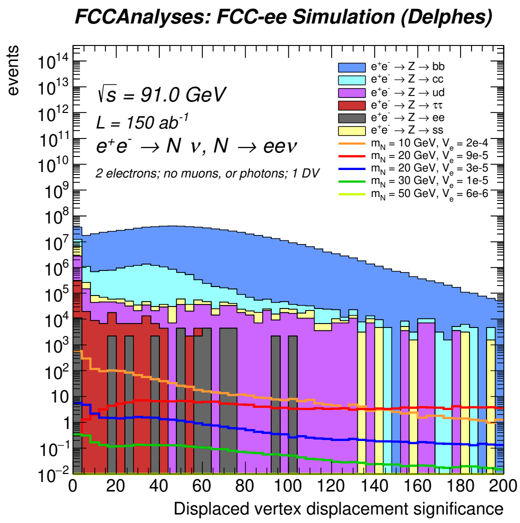

(c)

Figure 10: Distributions, normalised to 150 ab^{-1}, of the (a) reconstructed decay length, (b) the error in this quantity and (c) its significance, for background and benchmark HNL processes for events with exactly 2 electrons, no muons and photons and an additional requirement of exactly 1 reconstructed secondary vertex (reconstructed with a track p_T cut of 1 GeV and a minimum $|d_0|$ requirement of 0.5 mm).

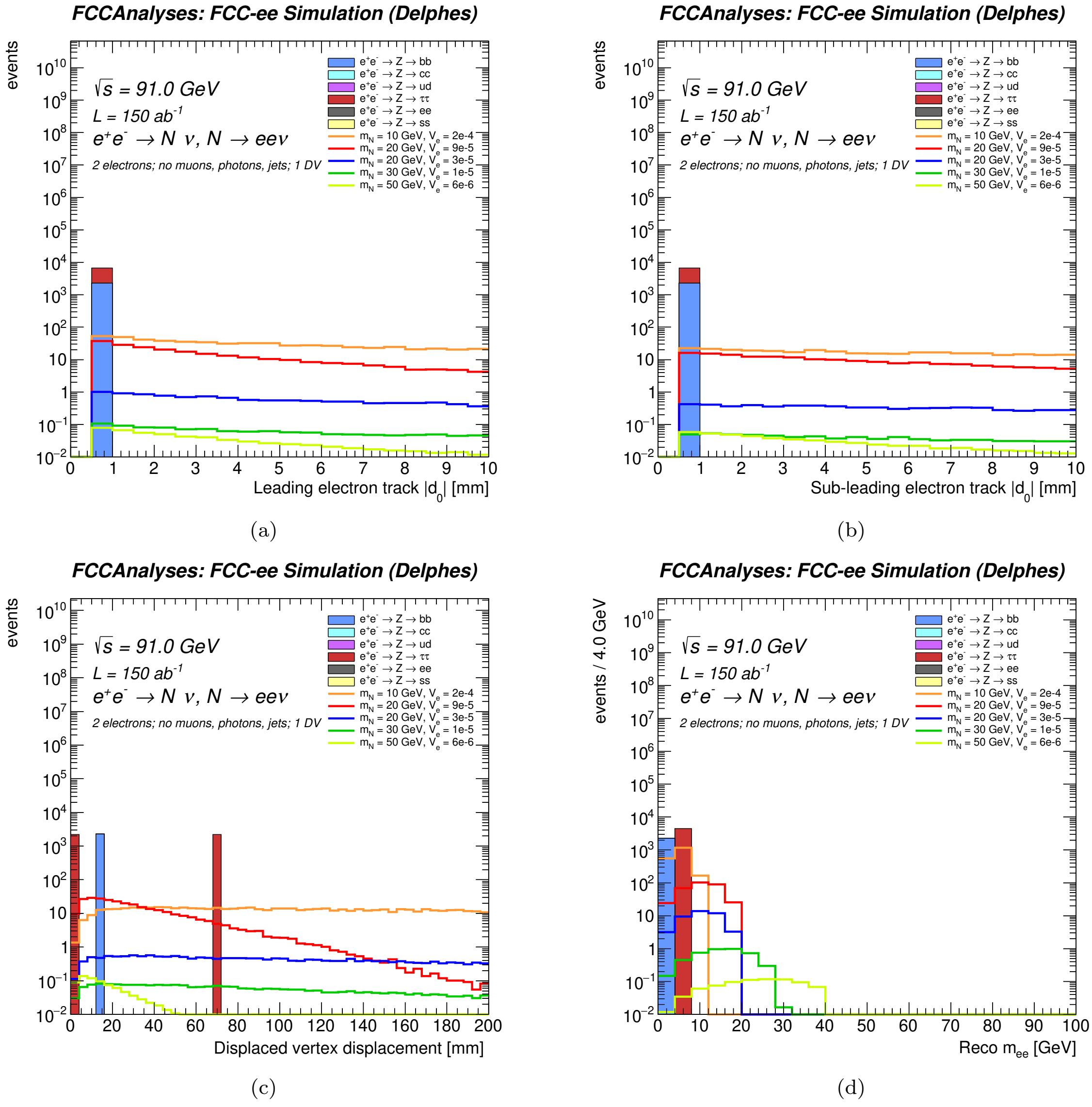

Figure 11: Distributions, normalised to 150 ab^{-1} for background and benchmark HNL processes for events with exactly 2 electrons, no muons, photons or jets and an additional requirement of exactly 1 reconstructed secondary vertex (reconstructed with a track p_T cut of 1 GeV and a minimum $|d_0|$ requirement of 0.5 mm). (a) and (b) show the leading and sub-leading electron track $|d_0|$, (c) shows the reconstructed decay length and (d) the invariant mass of the di-electron system.

5 Optimisation of secondary vertex reconstruction

The results in Section 4 demonstrated that placing a requirement of exactly one reconstructed secondary vertex provided significant background rejection. The choice of secondary vertex reconstruction algorithm, along with choices of the selected tracks used (p_T and $|d_0|$ requirements) could be further optimised to increase sensitivity to LLPs including HNLs.

To illustrate this, this section considers the impact of restricting tracks used in the secondary vertex reconstruction to those with $|d_0| > 2$ mm. Figure 12 shows distributions of the number of secondary vertices reconstructed in events with exactly two electrons, and no photons or muons. Comparing to Figure 6, no background processes have more than 2 secondary vertices, and the background rejection when selecting events with exactly one displaced vertex is an order of magnitude higher.

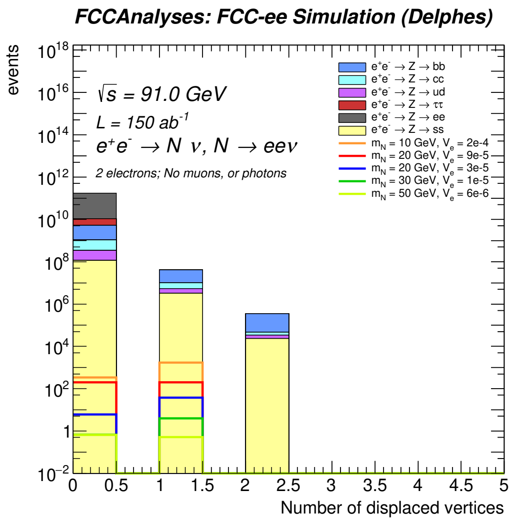

Figure 12: Distribution of the number of reconstructed secondary vertices (reconstructed with a track p_T cut of 1 GeV and a minimum $|d_0|$ requirement of 2 mm) , normalised to 150 ab^{-1}, for representative HNL benchmark points and the main Z-pole background processes. All events are required to have exactly two electrons, and no additional muons or photons.

Figure 13 shows the missing momentum, jet multiplicity, di-electron invariant mass and leading electron d_0 distributions for events with 2 electrons, no electrons or muons and exactly one reconstructed secondary vertex (using tracks with $|d_0| > 2$ mm). The jet multiplicity distribution shows that vetoing jets would remove all MC events from the backgrounds. This is further demonstrated in Table 5 which gives expected background yields, normalised to 150 ab^{-1} for the selections considered using the tighter secondary vertex requirement.

$Z \rightarrow$	2 electrons	Veto photons and muons	Veto photons and muons; 1 DV	Veto photons, muons, jets; 1 DV
ee	2.22e+11 ± 1.41e+09	2.22e+11 ± 2.58e+07	1.50e+04 ± 6.70e+03	≤ 6.70e+03
$\tau\tau$	7.37e+09 ± 2.60e+08	7.37e+09 ± 4.72e+06	2.42e+05 ± 2.71e+04	≤ 2.71e+04
bb	5.83e+09 ± 2.37e+08	5.83e+09 ± 4.25e+06	4.21e+07 ± 3.62e+05	≤ 3.62e+05
cc	1.01e+09 ± 6.80e+07	1.01e+09 ± 1.47e+06	6.52e+06 ± 1.18e+05	≤ 1.18e+05
ud	3.12e+08 ± 8.63e+07	3.12e+08 ± 1.23e+06	2.87e+06 ± 1.18e+05	≤ 1.18e+05
ss	1.62e+08 ± 2.72e+07	1.62e+08 ± 5.89e+05	4.49e+06 ± 9.80e+04	≤ 9.80e+04

Table 5: Event yields, normalised to $205ab^{-1}$ for Z-pole background processes for a baseline di-electron event selection involving vetoes on muons, photons and jets and requiring exactly 1 reconstructed secondary vertex (reconstructed with a track p_T cut of 1 GeV and a minimum $|d_0|$ requirement of 2 mm). The inequalities in the final column indicate that all MC events are removed by the full selection.

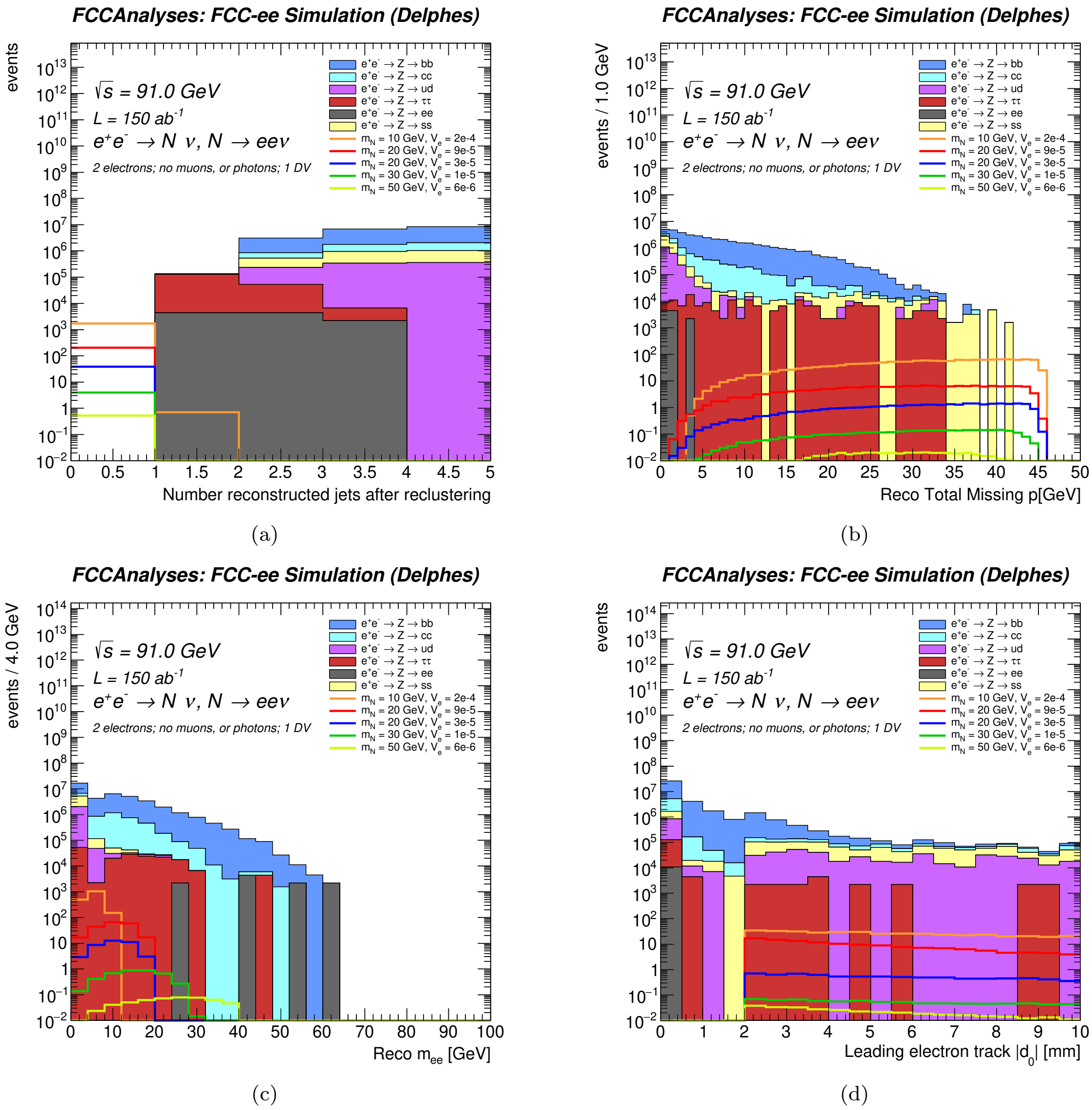

Figure 13: Distributions, normalised to 150 ab^{-1}, of the (a) the jet multiplicity, (b) magnitude of the missing momentum, (c) the di-electron invariant mass and (d) the leading electron $|d_0|$ for background and benchmark HNL processes for events with exactly 2 electrons, no muons and photons and an additional requirement of exactly 1 reconstructed secondary vertex (reconstructed with a track p_T cut of 1 GeV and a minimum $|d_0|$ requirement of 2 mm).

6 Sensitivity projections

This study will consider the same benchmark HNL signal scenario as in the Snowmass Paper [4]. This considered a type-I SeeSaw model with production and decay of a single HNL species. Whilst the more promising models compatible with external constraints include two or three HNLs in the same mass range or possibly degenerate, this was considered a reasonably starting point for considering experimental prospects.

The branching ratio to any light (anti-)neutrino and a HNL, N, which mixes with all three families is given by

$$\mathrm{BR}(Z \to \nu N) = \frac{2}{3}|U_N|^2 \mathrm{BR}(Z \to \text{invisible}) \left(1 + \frac{m_N^2}{2m_Z^2}\right)\left(1 - \frac{m_N^2}{m_Z^2}\right) \tag{1}$$

and charged current decay width in this scenario can be calculated as

$$\Lambda_N = \frac{1}{c\tau_N} \simeq C_0 C_{MD} |U_N|^2 \left(\frac{m_N}{50\ \mathrm{GeV}}\right)^5 \times \left(\frac{3 \times 10^9}{1\ \mathrm{cm}}\right), \tag{2}$$

where C_0 is a numerical coefficient of order 1 (and taken to be 1 in this study), C_{MD} depends on the Majorana or Dirac nature of the HNL ($C_{MD} = 1$ or 2 for Dirac and Majorana HNLs respectively) and $|U_N|^2 = \sum_{\ell=e,\mu,\tau} |U_{\ell N}|^2$. This study only considers couplings to electrons thus $|U_N|^2 = |V_{eN}|^2$.

To consider the possible sensitivity of a background-free search defined by requiring exactly two electrons, no muons, photons or jets and a displaced vertex reconstructed with a track p_T cut of 1 GeV and a minimum $|d_0|$ requirement of 2 mm), Table 6 provides event yields for a range of HNL benchmark points where the mass of the HNL and its coupling to electrons (V_{eN}) is varied. For simplicity, the couplings to other neutrino species are set to 0. In the final column the yields marked in bold are those of O(1) or higher, which indicate the potential for discovery in a background free search. The sample cross-sections, and calculated values for $c\tau N$ calculated using Equation 2 are also provided. For models with relatively high cross-sections, the lack of sensitivity can typically be attributed to a value of $c\tau_N$ so high that the HNL would pass out of the IDEA tracker without decaying, or too low such that a prompt search would be more suitable.

m_N [GeV], $\lvert V_{eN}\rvert$	$c\tau_N$ [cm] ($C_0 = 1$)	Cross-section [pb]	Expected events	2 electrons	Veto photons and muons	1 DV	Veto jets and 1 DV
10, 3×10^{-4}	5.7870	3.799×10^{-5}	5,698.62	6.36e+03 ± 1.24e+01	6.36e+03 ± 3.15e+01	4.74e+03 ± 2.72e+01	**4.74e+03 ± 2.72e+01**
10, 1×10^{-4}	52.0833	4.221×10^{-6}	633.19	4.97e+02 ± 3.86e-01	4.97e+02 ± 2.93e+00	4.24e+02 ± 2.71e+00	**4.23e+02 ± 2.71e+00**
10, 3×10^{-5}	578.7037	3.799×10^{-7}	56.99	6.67e+00 ± 4.02e-03	6.67e+00 ± 1.02e-01	5.58e+00 ± 9.32e-02	**5.57e+00 ± 9.31e-02**
10, 1×10^{-5}	5208.3333	4.221×10^{-8}	6.33	9.42e-02 ± 5.31e-05	9.42e-02 ± 4.04e-03	8.07e-02 ± 3.74e-03	8.03e-02 ± 3.73e-03
10, 3×10^{-6}	57870.3704	3.799×10^{-9}	0.57	7.01e-04 ± 4.12e-07	7.01e-04 ± 1.04e-04	5.92e-04 ± 9.60e-05	5.92e-04 ± 9.60e-05
10, 1×10^{-6}	520833.3333	4.221×10^{-10}	0.06	7.09e-02 ± 4.61e-07	7.09e-02 ± 3.50e-04	≤ 3.50e-04	≤ 3.50e-04
20, 3×10^{-4}	0.1808	3.387×10^{-5}	5,079.94	6.15e+03 ± 1.09e+01	6.15e+03 ± 2.92e+01	1.85e+02 ± 5.07e+00	**1.85e+02 ± 5.07e+00**
20, 1×10^{-4}	1.6276	3.763×10^{-6}	564.42	6.82e+02 ± 4.03e-01	6.82e+02 ± 3.24e+00	3.08e+02 ± 2.18e+00	**3.08e+02 ± 2.18e+00**
20, 3×10^{-5}	18.0845	3.387×10^{-7}	50.80	6.06e+01 ± 1.08e-02	6.06e+01 ± 2.90e-01	5.23e+01 ± 2.70e-01	**5.23e+01 ± 2.70e-01**
20, 1×10^{-5}	162.7604	3.764×10^{-8}	5.65	3.84e+00 ± 3.02e-04	3.84e+00 ± 2.43e-02	3.44e+00 ± 2.30e-02	**3.43e+00 ± 2.30e-02**
20, 3×10^{-6}	1808.4491	3.387×10^{-9}	0.51	4.52e-02 ± 2.95e-06	4.52e-02 ± 7.92e-04	4.00e-02 ± 7.46e-04	3.99e-02 ± 7.45e-04
20, 1×10^{-6}	16276.0417	3.765×10^{-10}	0.06	5.91e-04 ± 3.75e-08	5.91e-04 ± 3.02e-05	5.19e-04 ± 2.83e-05	5.17e-04 ± 2.83e-05
30, 3×10^{-4}	0.0238	3.007×10^{-5}	4,510.07	5.76e+03 ± 9.36e+00	5.76e+03 ± 2.67e+01	≤ 2.67e+01	≤ 2.67e+01
30, 1×10^{-4}	0.2143	3.341×10^{-6}	501.12	6.40e+02 ± 3.47e-01	6.40e+02 ± 2.96e+00	1.79e+01 ± 4.95e-01	**1.79e+01 ± 4.95e-01**
30, 3×10^{-5}	2.3815	3.007×10^{-7}	45.10	5.76e+01 ± 9.35e-03	5.76e+01 ± 2.66e-01	2.84e+01 ± 1.87e-01	**2.84e+01 ± 1.87e-01**
30, 1×10^{-5}	21.4335	3.341×10^{-8}	5.01	6.32e+00 ± 3.44e-04	6.32e+00 ± 2.94e-02	5.40e+00 ± 2.72e-02	**5.40e+00 ± 2.72e-02**
30, 3×10^{-6}	238.1497	3.007×10^{-9}	0.45	3.44e-01 ± 7.23e-06	3.44e-01 ± 2.06e-03	3.14e-01 ± 1.97e-03	3.13e-01 ± 1.97e-03
30, 1×10^{-6}	2143.3471	3.341×10^{-10}	0.05	3.44e-01 ± 7.23e-06	3.44e-01 ± 2.06e-03	3.14e-01 ± 1.97e-03	3.13e-01 ± 1.97e-03
40, 3×10^{-4}	0.0057	2.569×10^{-5}	3,854.11	4.99e+03 ± 7.44e+00	4.99e+03 ± 2.29e+01	≤ 2.29e+01	≤ 2.29e+01
40, 1×10^{-4}	0.0509	2.855×10^{-6}	428.24	5.55e+02 ± 2.76e-01	5.55e+02 ± 2.55e+00	≤ 2.55e+00	≤ 2.55e+00
40, 3×10^{-5}	0.5651	2.569×10^{-7}	38.54	4.99e+01 ± 7.44e-03	4.99e+01 ± 2.29e-01	5.23e+00 ± 7.43e-02	**5.23e+00 ± 7.43e-02**
40, 1×10^{-5}	5.0863	2.855×10^{-8}	4.28	5.54e+00 ± 2.75e-04	5.54e+00 ± 2.55e-02	3.28e+00 ± 1.96e-02	**3.28e+00 ± 1.96e-02**
40, 3×10^{-6}	56.5140	2.569×10^{-9}	0.39	4.87e-01 ± 7.35e-06	4.87e-01 ± 2.26e-03	4.32e-01 ± 2.13e-03	4.31e-01 ± 2.13e-03
40, 1×10^{-6}	508.6263	2.855×10^{-10}	0.04	2.76e-02 ± 1.94e-07	2.76e-02 ± 1.80e-04	2.49e-02 ± 1.71e-04	2.48e-02 ± 1.70e-04
50, 3×10^{-4}	0.0019	2.054×10^{-5}	3,080.85	4.01e+03 ± 5.33e+00	4.01e+03 ± 1.84e+01	≤ 1.84e+01	≤ 1.84e+01
50, 1×10^{-4}	0.0167	2.282×10^{-6}	342.34	4.46e+02 ± 1.98e-01	4.46e+02 ± 2.04e+00	≤ 2.04e+00	≤ 2.04e+00
50, 3×10^{-5}	0.1852	2.054×10^{-7}	30.81	4.01e+01 ± 5.33e-03	4.01e+01 ± 1.84e-01	6.06e-02 ± 7.15e-03	6.06e-02 ± 7.15e-03
50, 1×10^{-5}	1.6667	2.282×10^{-8}	3.42	4.46e+00 ± 1.98e-04	4.46e+00 ± 2.04e-02	9.89e-01 ± 9.62e-03	9.89e-01 ± 9.62e-03
50, 3×10^{-6}	18.5185	2.054×10^{-9}	0.31	4.00e-01 ± 5.32e-06	4.00e-01 ± 1.83e-03	2.68e-01 ± 1.50e-03	2.68e-01 ± 1.50e-03
50, 1×10^{-6}	166.6667	2.282×10^{-10}	0.03	4.14e-02 ± 1.90e-07	4.14e-02 ± 1.97e-04	3.35e-02 ± 1.77e-04	3.35e-02 ± 1.77e-04
60, 3×10^{-4}	0.0007	1.479×10^{-5}	2,218.02	2.89e+03 ± 3.26e+00	2.89e+03 ± 1.32e+01	≤ 1.32e+01	≤ 1.32e+01
60, 1×10^{-4}	0.0067	1.643×10^{-6}	246.45	3.21e+02 ± 1.21e-01	3.21e+02 ± 1.47e+00	≤ 1.47e+00	≤ 1.47e+00
60, 3×10^{-5}	0.0744	1.479×10^{-7}	22.18	2.89e+01 ± 3.26e-03	2.89e+01 ± 1.32e-01	≤ 1.32e-01	≤ 1.32e-01
60, 1×10^{-5}	0.6698	1.643×10^{-8}	2.46	3.21e+00 ± 1.21e-04	3.21e+00 ± 1.47e-02	6.16e-02 ± 2.04e-03	6.16e-02 ± 2.04e-03
60, 3×10^{-6}	7.4422	1.479×10^{-9}	0.22	2.89e-01 ± 3.26e-06	2.89e-01 ± 1.32e-03	9.94e-02 ± 7.76e-04	9.94e-02 ± 7.76e-04
60, 1×10^{-6}	66.9796	1.643×10^{-10}	0.02	3.18e-02 ± 1.20e-07	3.18e-02 ± 1.46e-04	1.86e-02 ± 1.12e-04	1.86e-02 ± 1.12e-04
70, 3×10^{-4}	0.0003	8.907×10^{-6}	1,336.10	1.74e+03 ± 1.52e+00	1.74e+03 ± 7.98e+00	≤ 7.98e+00	≤ 7.98e+00
70, 1×10^{-4}	0.0031	9.898×10^{-7}	148.47	1.93e+02 ± 5.65e-02	1.93e+02 ± 8.86e-01	≤ 8.86e-01	≤ 8.86e-01
70, 3×10^{-5}	0.0344	8.907×10^{-8}	13.36	1.74e+01 ± 1.52e-03	1.74e+01 ± 7.98e-02	≤ 7.98e-02	≤ 7.98e-02
70, 1×10^{-5}	0.3099	9.898×10^{-9}	1.48	1.93e+00 ± 5.65e-05	1.93e+00 ± 8.86e-03	≤ 8.86e-03	≤ 8.86e-03
70, 3×10^{-6}	3.4432	8.907×10^{-10}	0.13	1.74e-01 ± 1.52e-06	1.74e-01 ± 7.98e-04	1.48e-02 ± 2.32e-04	1.48e-02 ± 2.32e-04
70, 1×10^{-6}	30.9891	9.898×10^{-11}	0.01	1.93e-02 ± 5.64e-08	1.93e-02 ± 8.86e-05	6.69e-03 ± 5.21e-05	6.69e-03 ± 5.21e-05
80, 3×10^{-4}	0.0002	2.118×10^{-5}	3,177.04	3.98e+03 ± 5.48e+00	3.98e+03 ± 1.86e+01	≤ 1.86e+01	≤ 1.86e+01
80, 1×10^{-4}	0.0016	2.353×10^{-6}	353.00	4.42e+02 ± 2.03e-01	4.42e+02 ± 2.06e+00	≤ 2.06e+00	≤ 2.06e+00
80, 3×10^{-5}	0.0177	2.118×10^{-7}	31.77	3.97e+01 ± 5.47e-03	3.97e+01 ± 1.86e-01	≤ 1.86e-01	≤ 1.86e-01
80, 1×10^{-5}	0.1589	2.353×10^{-8}	3.53	4.42e+00 ± 2.03e-04	4.42e+00 ± 2.06e-02	9.65e-05 ± 9.65e-05	9.65e-05 ± 9.65e-05
80, 3×10^{-6}	1.7661	2.118×10^{-9}	0.32	3.97e-01 ± 5.47e-06	3.97e-01 ± 1.86e-03	2.38e-02 ± 4.54e-04	2.38e-02 ± 4.54e-04
80, 1×10^{-6}	15.8946	2.353×10^{-10}	0.04	4.41e-02 ± 2.03e-07	4.41e-02 ± 2.06e-04	1.31e-02 ± 1.12e-04	1.31e-02 ± 1.12e-04
90, 3×10^{-4}	0.0001	7.917×10^{-8}	11.88	1.55e+01 ± 1.28e-03	1.55e+01 ± 7.09e-02	≤ 7.09e-02	≤ 7.09e-02
90, 1×10^{-4}	0.0009	8.797×10^{-9}	1.32	1.72e+00 ± 4.73e-05	1.72e+00 ± 7.88e-03	≤ 7.88e-03	≤ 7.88e-03
90, 3×10^{-5}	0.0098	7.917×10^{-10}	0.12	1.55e-01 ± 1.28e-06	1.55e-01 ± 7.10e-04	≤ 7.10e-04	≤ 7.10e-04
90, 1×10^{-5}	0.0882	8.797×10^{-11}	0.01	1.72e-02 ± 4.73e-08	1.72e-02 ± 7.88e-05	≤ 7.88e-05	≤ 7.88e-05
90, 3×10^{-6}	0.9800	7.917×10^{-12}	< 0.01	1.55e-03 ± 1.28e-09	1.55e-03 ± 7.09e-06	≤ 7.09e-06	≤ 7.09e-06
90, 1×10^{-6}	8.8204	8.797×10^{-13}	< 0.01	1.72e-04 ± 4.73e-11	1.72e-04 ± 7.88e-07	≤ 7.88e-07	≤ 7.88e-07

Table 6: Event yields, normalised to $150ab^{-1}$ for HNL signal points for a baseline di-electron event selection involving vetoes on muons, photons and jets and requiring exactly 1 reconstructed secondary vertex (reconstructed with a track p_T cut of 1 GeV and a minimum $|d_0|$ requirement of 2 mm). In the final column, the numbers marked in bold illustrate scenarios where this selection would yield at least O(1) signal events, and thus could be discovered at FCC-ee assuming a background-free search.

In order to illustrate the sensitivity in comparison to Figure 2, Figure 14 shows the 3-event contour for this initial selection using the signal events included in Table 6 but scaled to the updated Z-pole luminosity corresponding to 6×10^{12} Z bosons, compared to a selection of constraints from future experiments compiled through the work of Ref. [14].

The FCC-ee projections presented here should be seen as conservative for a number of reasons. Firstly- only the leptonic HNL decay is considered- including the semi-leptonic decays would enable more direct comparison with previous limits. Secondly, the limited MC statistics mean that the event selection criteria are not heavily optimised. This is left for future study. Despite this, there are regions at higher masses and larger couplings where the constraints from this study extend beyond the previous FCC-ee line in Figure 2, which motivates further detailed projections that combine all HNL decay channels.

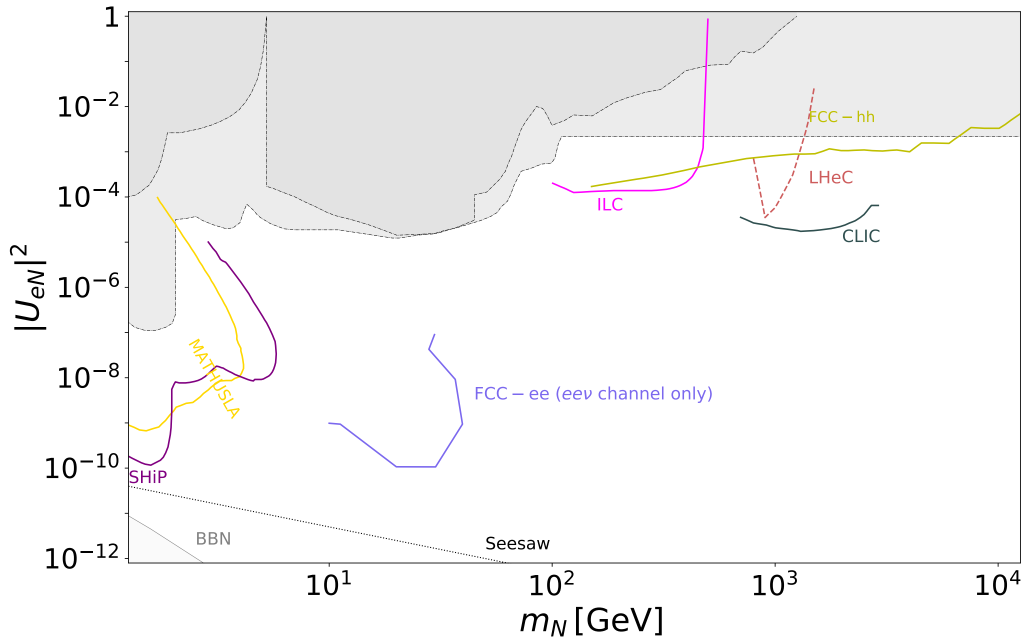

Figure 14: Comparison of the 3-event contour for the selection outlined in this study assuming a background-free search with signal yields normalised to 6×10^{12} Z bosons, compared to a selection of collider (and other) constraints compiled through the work of Ref. [14], as a function of the HNL mass and the electron-neutrino coupling, for the signal points displayed in Table 6

7 Conclusions and outlook

This note has considered updated studies of the sensitivity of the Z-pole run at FCC-ee to Heavy Neutral Leptons with dominant couplings to the electron. Updated MC samples have been used to investigate an event selection requiring exactly two electrons, a veto on additional muons, jets and photons and exactly one reconstructed secondary vertex (reconstructed with a track p_T cut of 1 GeV and a minimum $|d_0|$ requirement of 2 mm). Under the assumption that this selection would be background free the projected sensitivity is compared to previous FCC-ee projections (that assumed 100% signal efficiency and background-free search conditions under particular HNL scenarios). These results provide updated estimates of signal acceptances in displaced vertex signatures, and are consistent with previous projections accounting for the lack of inclusion of the semi-leptonic decay channel in this study, and exceed previous limits for some models with smaller couplings and higher HNL masses. Kinematic distributions of additional variables including angular distributions are presented for various benchmark HNL scenarios that could be further studied as a source of additional background discrimination or to characterise a potential signal. These results motivate further optimisation of the search strategy with larger MC background samples and calculations of the expected sensitivity when the di-electron and semileptonic channels are combined.

References

[1] R. K. Ellis et al. "Physics Briefing Book: Input for the European Strategy for Particle Physics Update 2020". In: (Oct. 2019). arXiv: 1910.11775 [hep-ex].

[2] S. Antusch, E. Cazzato, and O. Fischer. "Displaced vertex searches for sterile neutrinos at future lepton colliders". In: *JHEP* 12 (2016), p. 007. DOI: 10.1007/JHEP12(2016)007. arXiv: 1604.02420 [hep-ph].

[3] H. Abramowicz et al. "The International Linear Collider Technical Design Report - Volume 4: Detectors". In: (June 2013). Ed. by T. Behnke, J. E. Brau, P. N. Burrows, J. Fuster, M. Peskin, M. Stanitzki, Y. Sugimoto, S. Yamada, and H. Yamamoto. arXiv: 1306.6329 [physics.ins-det].

[4] A. Blondel et al. "Searches for long-lived particles at the future FCC-ee". In: *Front. in Phys.* 10 (2022), p. 967881. DOI: 10.3389/fphy.2022.967881. arXiv: 2203.05502 [hep-ex].

[5] J. Alwall, R. Frederix, S. Frixione, V. Hirschi, F. Maltoni, O. Mattelaer, H. .-. Shao, T. Stelzer, P. Torrielli, and M. Zaro. "The automated computation of tree-level and next-to-leading order differential cross sections, and their matching to parton shower simulations". In: *JHEP* 07 (2014), p. 079. DOI: 10.1007/JHEP07(2014)079. arXiv: 1405.0301 [hep-ph].

[6] C. Bierlich et al. "A comprehensive guide to the physics and usage of PYTHIA 8.3". In: *SciPost Phys. Codeb.* 2022 (2022), p. 8. DOI: 10.21468/SciPostPhysCodeb.8. arXiv: 2203.11601 [hep-ph].

[7] J. de Favereau, C. Delaere, P. Demin, A. Giammanco, V. Lemaıtre, A. Mertens, and M. Selvaggi. "DELPHES 3, A modular framework for fast simulation of a generic collider experiment". In: *JHEP* 02 (2014), p. 057. DOI: 10.1007/JHEP02(2014)057. arXiv: 1307.6346 [hep-ex].

[8] A. Abada et al. "FCC-ee: The Lepton Collider: Future Circular Collider Conceptual Design Report Volume 2". In: *Eur. Phys. J. ST* 228.2 (2019), pp. 261–623. DOI: 10.1140/epjst/e2019-900045-4.

[9] M. Cacciari, G. P. Salam, and G. Soyez. "FastJet User Manual". In: *Eur. Phys. J. C* 72 (2012), p. 1896. DOI: 10.1140/epjc/s10052-012-1896-2. arXiv: 1111.6097 [hep-ph].

[10] F. Gaede, T. Madlener, P. Declara Fernandez, G. Ganis, B. Hegner, C. Helsens, A. Sailer, G. A Stewart, and V. Voelkl. "EDM4hep - a common event data model for HEP experiments". In: *PoS* ICHEP2022 (2022), p. 1237. DOI: 10.22323/1.414.1237. URL: https://cds.cern.ch/record/2869508.

[11] M. Cacciari, G. P. Salam, and G. Soyez. "The anti-k_t jet clustering algorithm". In: *JHEP* 04 (2008), p. 063. DOI: 10.1088/1126-6708/2008/04/063. arXiv: 0802.1189 [hep-ph].

[12] S. Weinzierl. "Jet algorithms in electron-positron annihilation: Perturbative higher order predictions". In: *Eur. Phys. J. C* 71 (2011). [Erratum: Eur.Phys.J.C 71, 1717 (2011)], p. 1565. DOI: 10.1140/epjc/s10052-011-1717-z. arXiv: 1011.6247 [hep-ph].

[13] T. Suehara and T. Tanabe. "LCFIPlus: A Framework for Jet Analysis in Linear Collider Studies". In: *Nucl. Instrum. Meth. A* 808 (2016), pp. 109–116. DOI: 10.1016/j.nima.2015.11.054. arXiv: 1506.08371 [physics.ins-det].

[14] P. D. Bolton, F. F. Deppisch, and P. S. Bhupal Dev. "Neutrinoless double beta decay versus other probes of heavy sterile neutrinos". In: *JHEP* 03 (2020), p. 170. DOI: 10.1007/JHEP03(2020)170. arXiv: 1912.03058 [hep-ph].